REPORT DOCUMENTATION PAGE

AFRL-SR-BL-TR-01-

0347

Public reporting burden for this collection of information is estimated to average 1 hour per response, including the time for reviewing instructions, searching existing data sources, gathering and maintaining the data needed, and completing and reviewing the collection of information. Send comments regarding this burden estimate or any other aspect of this collection of information, including suggestions for reducing this burden, to Washington Headquarters Services, Directorate for information Operations and Reports, 1215 Jefferson Davis Highway, Suite 1204, Arlington, VA 22202-4302, and to the Office of Management and Budget, Paperwork Reduction Project (0704-0188), Washington, DC 20503.

1. AGENCY USE ONLY *(Leave blank)*	2. REPORT DATE	3. REPORT TYPE AND DATES COVERED
	18 MAY	FINAL REPORT: 1 OCT 97 TO 30 SEPT 00

4. TITLE AND SUBTITLE
TURBULENT SPOT CHARACTERIZATION AND THE MODELING OF TRANSITIONAL HEAT TRANSFER IN TURBINES

5. FUNDING NUMBERS
F49620-97-1-0524

6. AUTHOR(S)
JOHN E. LAGRAFF

7. PERFORMING ORGANIZATION NAME(S) AND ADDRESS(ES)
SYRACUSE UNIVERSITY
OFFICE OF SPONSORED PROGRAMS
113 BOWNE HALL/SYRACUSE, NEW YORK 13244-1200

8. PERFORMING ORGANIZATION REPORT NUMBER

9. SPONSORING/MONITORING AGENCY NAME(S) AND ADDRESS(ES)
AFOSR/NA
801 N. RANDOLPH ST. SUITE 732
ARLINGTON VA 22203-1977

10. SPONSORING/MONITORING AGENCY REPORT NUMBER

11. SUPPLEMENTARY NOTES

12a. DISTRIBUTION AVAILABILITY STATEMENT
APPROVED FOR PUBLIC RELEASE: DISTRIBUTION IS UNLIMITED

12b. DISTRIBUTION CODE

AIR FORCE OFFICE OF SCIENTIFIC RESEARCH (AFOSR)
NOTICE OF TRANSMITTAL DTIC. THIS TECHNICAL REPORT
HAS BEEN REVIEWED AND IS APPROVED FOR PUBLIC RELEASE
LAW AFR 190-12. DISTRIBUTION IS UNLIMITED.

13. ABSTRACT *(Maximum 200 words)*

OPTIMUM DESIGN OF GAS TURBINE BLADES DEPENDS ON ACCURATE PREDICTION OF BOUNDARY LAYER TRANSITION. THE PURPOSE OF THIS RESEARCH IS TO OBTAIN MORE INFORMATION ON THE GENERATION, PROPAGATION, AND COALESCENCE ON TURBULENT SPOTS IN A TRANSITIONAL BOUNDARY LAYER, AND EXAMINE THE EFFECTS OF FREESTREAM TURBULENCE, PRESSURE GRADIENT, AND CROSSFLOW. EXPERIMENTAL DATA FROM THIS STUDY MAY BE USED TO IMPROVE EXISTING CFD MODELS, ALLOWING DESIGNERS TO MAKE MORE ACCURATE PREDICTIONS OF TRANSITIONAL HEAT TRANSFER IN TURBINES.

20010604 131

14. SUBJECT TERMS	15. NUMBER OF PAGES
TURBULENT SPOT CHARACTERIZATION AND THE MODELING OF TRANSITIONAL HEAT TRANSFER IN TURBINES	16. PRICE CODE

17. SECURITY CLASSIFICATION OF REPORT	18. SECURITY CLASSIFICATION OF THIS PAGE	19. SECURITY CLASSIFICATION OF ABSTRACT	20. LIMITATION OF ABSTRACT
UNCLASSIFIED	UNCLASSIFIED	UNCLASSIFIED	UL

TURBULENT SPOT CHARACTERIZATION AND THE MODELING OF TRANSITIONAL HEAT TRANSFER IN TURBINES

Final Report

October 1, 1997 – September 30, 2000

AFSOR Grant Number F49620-97-1-0524

John E. LaGraff
Department of Mechanical, Aerospace, and Manufacturing Engineering
Syracuse University, New York
April 2, 2001

Abstract

Optimum design of gas turbine blades depends on accurate prediction of boundary layer transition. The purpose of this research is to obtain more information on the generation, propagation, and coalescence of turbulent spots in a transitional boundary layer, and examine the effects of freestream turbulence, pressure gradient, and crossflow. Experimental data from this study may be used to improve existing CFD models, allowing designers to make more accurate predictions of transitional heat transfer in turbines.

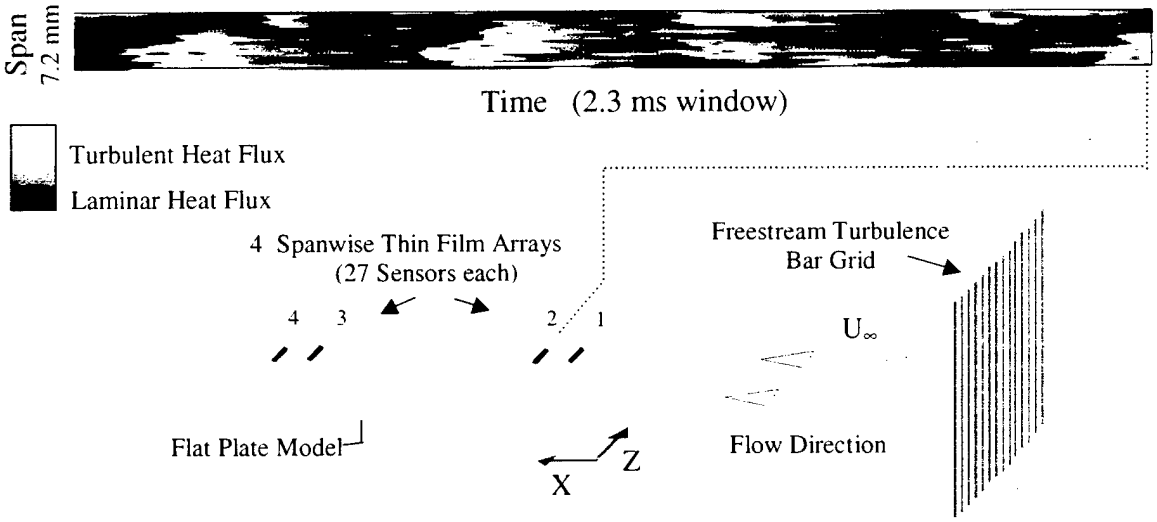

Figure 1 Experimental setup showing the flat plate wind tunnel model instrumented with high-density thin film arrays. The spanwise arrays shown are perpendicular to the flow direction. The top image is a view of transitional heat flux in the *z-t* plane from array #2 which shows the heat flux events crossing a 9.6 mm span in less than 4.5 ms. The high frequency, high spatial resolution measurements are used to capture turbulent spot detail in a high speed transitional boundary layer.

Introduction

Accurate heat transfer predictions for the transition region between laminar and turbulent flow are critical to the turbine blade designer since up to 50% of the blade chord length may undergo transition. A key to modelling boundary layer transition is to incorporate knowledge of the generation, propagation, and coalescence of turbulent spots. Formation of an accurate transition model, which can be used to significantly improve CFD codes, relies on experimental measurement of actual turbulent spot characteristics under the influence of various disturbances.

Previous AFOSR supported work by a team of Syracuse University and Oxford University researchers and using the unique experimental facilities at Oxford University have provided a wealth of information on turbulent spot characteristics (Clark 1993, Hofeldt 1997). The effects of Mach number and acceleration parameter on turbulent spot celerities and spreading angle have been quantified, and measurements have been made to estimate the rate of natural spot generation. Precise measurement of the latter parameter, however, has proven to be rather difficult. Unlike the other spot parameters, generation rate does not address the characteristics of a single spot, but rather applies to the masses of spots produced over an entire transition area. The precise streamwise location of natural spot generation is unsteady and the spanwise locations are random. Newly developed spots are small, and detailed measurements therefore require high-resolution instrumentation.

Transition and turbulent spot development in turbines is still not fully understood. More fundamental experimental data is needed. Capturing turbulent spot generation rate detail in a high-speed transitional boundary layer through their effect on wall heat flux requires the resolution of very small, and very fast, surface heat flux events. This has proved possible using new high frequency, high-resolution thin film heat transfer gauge arrays developed at Oxford specifically for this study. Turbine boundary layers are influenced by a mix of disturbances including freestream turbulence, varying pressure gradient, and three-dimensional crossflow. The experimental program described in this report aims to study how each of these affect turbulent spot development and surface heat flux. A goal of the research is to provide new information that may improve prediction of transitional heat flux in turbines.

Instrumentation

Detailed measurements of high frequency heat transfer events require many closely spaced heat transfer sensors. High frequency response (200kHz), high resolution (0.2 mm spacing) thin film gauge arrays have been developed for resolving individual turbulent spot events. A full explanation of the high density thin film arrays, signal conditioning electronics, and heat flux data processing is explained in Anthony et. al. (1999). This section gives a brief description of the thin film arrays.

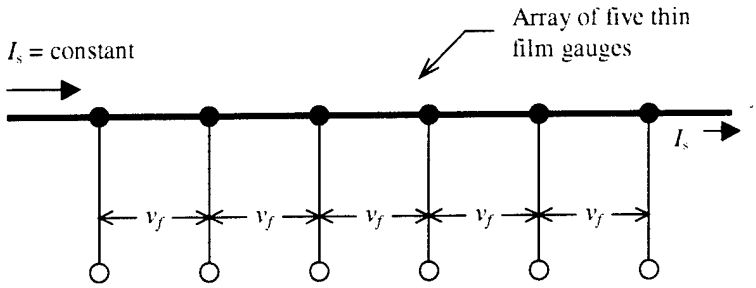

Figure 2 Simple diagram of a Thin Film Gauge Array with five sensing elements.

A simple sketch of a thin film sensor array is shown in Figure 2. The films are made of platinum and have a temperature sensitive resistance. The diagram shows five thin film sensors in series supplied with a constant current I_s. Changes in surface temperature are thus given by changes in the differential voltage drop v_f across the film. Low noise differential amplifiers are used to obtain the temperature signal from each sensor in the array. A digital filtering technique is then used to convert the recorded surface temperature into heat flux. The signal processing is described in the next section. The thin film gauge arrays have the following advantages:

- It is possible to align several gauges directly next to each other end to end.
- The voltage leads can be as thin as possible taking up significantly less surface space. Since virtually no current flows though the voltage leads (high input impedance amplifiers are used), their resistance is not critical to the measurement. An excessively high lead resistance, however, will contribute thermal noise to the measurement.
- The entire layout, leads and gauges, is just one layer of a single material. There is no need for the leads to be a separate low resistance metal such as copper, and the manufacturing process is much simpler.
- Only one constant current supply is needed to power several gauges. This greatly reduces the number of electronic components required for a given number of gauges.

A disadvantage of the new high-density array is that, as one end of the gauge is no longer at ground potential, differential amplifiers must be used to measure individual gauge voltages.

The thin film gauge arrays are manufactured using standard sputtering and photo-etching techniques to create a completely platinum sensor and lead pattern. The platinum thin film arrays are sputtered onto a thin flexible sheet of polyimide that is 50 microns thick.

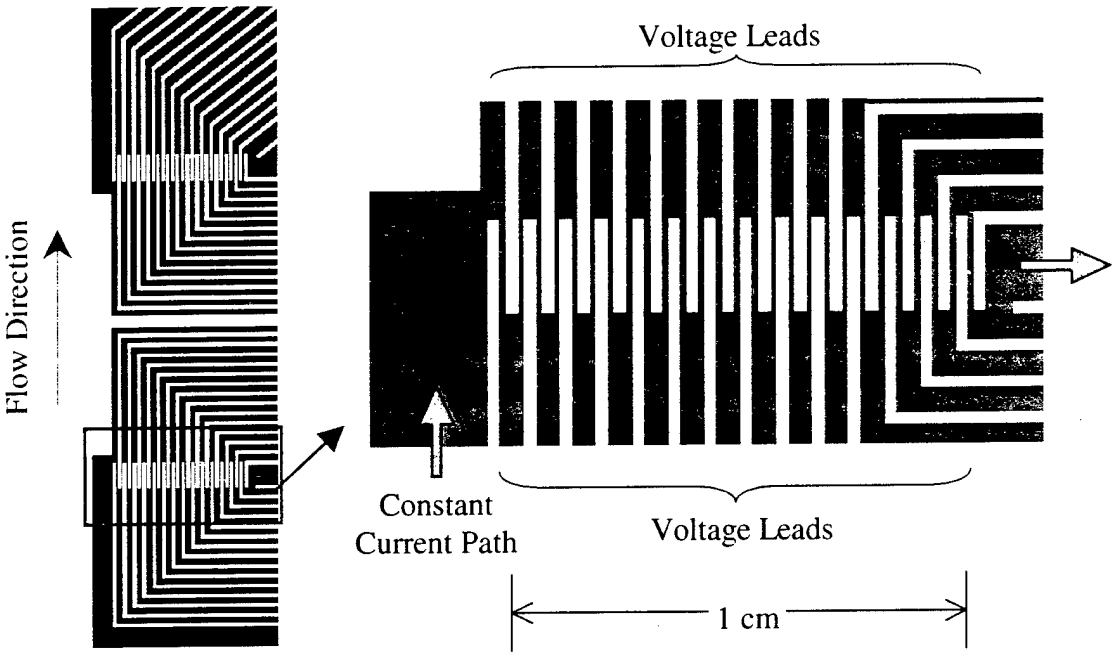

Figure 3 Magnified image of two high density platinum thin film arrays aligned in the spanwise direction (perpendicular to the flow). Each array consists of 27 sensors. The platinum is shown dark and the substrate is shown light.

This flexible sheet of sensors can then be glued onto test surfaces, such as turbine blades, to obtain high frequency, high spatial resolution surface heat flux data.

A magnified section of the platinum film layout used in this experiment is shown in Figure 3. The photo includes two high density arrays aligned in the spanwise direction, perpendicular to the flow. The magnified view of array #1 shows how current enters the array at the left, cascades through all the gauges, and leaves to the right. Voltage taps are taken off the ends of each film and passed through differential amplifiers. Closely spaced sensors like these can be used to form "images" of the surface heat flux events crossing the span of the array.

Signal Processing Technique

Signal processing to obtain the surface heat flux is broken into two parts. First, analog circuitry must condition the very small differential voltage fluctuations from the thin film to a high level signal that can be faithfully digitized by an A/D converter with adequate resolution. Second, digital signal processing algorithms are used to convert the temperature data to surface heat flux assuming 1-D heat conduction into a semi-infinite medium.

The natural frequency response of a gauge on a semi-infinite substrate decreases inversely with the square root of frequency (Schultz and Jones 1973). The approximate –10 dB/decade slope in the response attenuates high frequency information. High

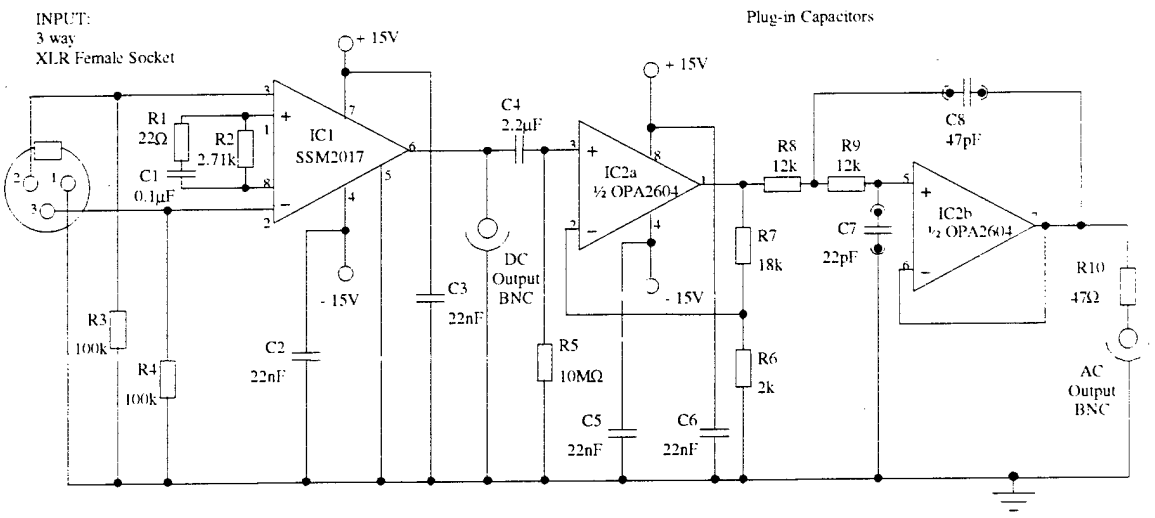

Figure 4 Single Channel of Thin Film Gauge Array Signal Conditioning Unit

frequency events such as blade wake passing and turbulent spots, which may occur at over 10kHz, are vulnerable to discretization error during digitization. To prevent this high frequency information from being swamped in digitization noise, a pre-emphasis filter is used to preferentially amplify the high frequency end prior to A/D conversion.

The pre-emphasis circuit is based on a low noise, low distortion differential instrumentation amplifier. The circuit diagram is given in Figure 4. The circuit rejects the common mode voltage fluctuation, and only amplifies the voltage *difference* between both ends of the gauge. The high frequency boost is obtained by replacing the gain setting resistance of the instrumentation amplifier (IC1 in Figure 4) with a frequency dependent impedance circuit (R_1C_1 & R_2 in Figure 4). The gain as a function of frequency through this section is given by the equation

$$G(j\omega) = 1 + \frac{2R_2}{R_g}\left(\frac{1 + j\omega C_g(R_1 + R_2)}{1 + j\omega C_g R_2}\right) \qquad (1)$$

where R_2 is an internal resistance of the instrumentation amplifier. The rest of the circuit includes a DC output, an AC coupling filter C4R5, 10X gain AC amplifier (IC2a), and an anti-alias low-pass filter (IC2b). These follow the pre-emphasis section and further condition the signal for analogue-to-digital conversion.

The output from the signal conditioning unit is sampled by multi-channel analog-to-digital (A/D) converters and passed to a PC where custom made Matlab software converts the data to heat flux. First, the time varying component of the thin-film voltage signal v_f is recovered by dividing by the signal conditioning gain and de-emphasizing it with a digital Infinite Impulse Response (IIR) filter having the inverse response to Equation (1). Once the voltage is recovered, the change in surface temperature is then given by

$$T = \frac{v_f}{\alpha_R V_0} \tag{2}$$

where V_0 is the dc voltage across the film at T_0, and α_R is the temperature coefficient of resistance for the thin film which is determined by calibration.

For a semi-infinite substrate under the thin film, the time-varying heat transfer rate q is given in frequency space by

$$q = \left(\sqrt{\rho c k}\sqrt{j\omega}\right) T \tag{3}$$

where $\rho c k$ is the product of the density, specific heat and thermal conductivity of the substrate material (Schultz and Jones 1973). The continuous $\sqrt{j\omega}$ frequency characteristic required by Equation 3 is approximated by an IIR filter having multiple, alternate, real poles and zeros spaced evenly on a logarithmic frequency scale. In the Laplace domain, the filter is

$$H(s) = \frac{q(s)}{T(s)} = A\frac{(s-z_1)(s-z_2)\cdots(s-z_{2n})}{(s-p_1)(s-p_2)\cdots(s-p2_{2n})} \tag{4}$$

where there are $2n$ poles and $2n$ zeros. The smallest in magnitude is the zero z_1, and subsequent poles and zeros are given by

$$p_1 = rz_1 \quad \text{and then} \quad z_i = rp_{i-1},\ p_i = rz_i \quad \text{for } i = 2,\cdots,2n.$$

and the largest pole is set at the Nyquist frequency. The cascaded filters give a "staircase" frequency characteristic that is a good approximation to the $\sqrt{j\omega}$ required. A custom Matlab program designs the IIR filters with the required characteristics. The cascaded filters are then applied to the temperature signal to obtain surface heat flux.

A typical 12 zero, 12 pole filter designed for a 400 kHz sampling rate has a frequency response accurate to better than 1 % over the range 0.02 Hz to 80 kHz. The time response to a $T \sim \sqrt{t}$ input (this should ideally give a step output) is accurate to better than 1 % over the time range 10 μs to 1.0 s. This method of transforming the time varying temperature signal into surface heat flux is computationally more efficient than previous methods due to the use of relatively small IIR filters. A guide to using these heat flux filtering methods is described in Oldfield (2000).

Experimental Set-up

Fundamental studies of boundary layer transition were performed on a 332mm x 150mm x 10mm Perspex flat plate model covered with a sheet of platinum thin film arrays. A total of 233 heat flux sensors were located on the surface in various arrays aligned in both spanwise and streamwise directions. The instrumented flat plate was installed in a high speed wind tunnel to obtain detailed transitional heat flux measurements.

Figure 5 shows a simple sketch of the flat plate experiment. Locations of only four spanwise arrays are shown for simplicity. Transient heat flux is driven by a temperature difference between the freestream airflow and the model. The duration of the tests were typically just under 0.3 sec allowing an assumption of 1-D semi-infinite heat transfer into the 10mm thick Perspex plate. Flow Mach numbers ranged from Mach 0.1 to Mach 0.4. To study the effects of turbulence, parallel bar grids were placed upstream of the model to generate freestream turbulence. Bar diameters of 4mm, 6mm, and 15mm were used to vary the turbulence intensity. The upstream location of the grid was adjusted to hold the integral turbulent length scale approximately constant while varying turbulence intensity (Roach 1987). To study the effects of pressure gradient, variable adverse and favorable pressure gradients were imposed with adjustable test section walls. The effects of crossflow were also studied using a specially contoured sidewall, which turns the flow across the span of the plate creating a skewed 3-D boundary layer.

Figure 5 332mm x 150mm x 10mm Plexi-glass flat plate model covered with a flexible, 50μm thick sheet of polyimide. 233 platinum sensors are sputtered onto the surface for high resolution turbulent spot measurements.

Figure 6 Turbulent spot heat flux images in the z-t plane (z is spanwise distance and t is time). The image shows surface heat flux events crossing a 40 mm span in less than 15 ms.

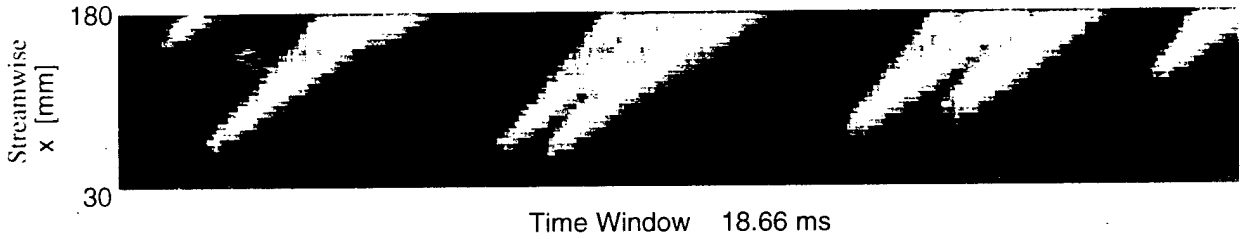

Figure 7 Turbulent spot heat flux images in the x-t plane taken from a streamwise array used to track growth and development of spots as they convect down the model surface.

Transitional Heat Flux Imaging

A high speed heat flux imaging technique is used to obtain the size and shape of individual, naturally-occurring turbulent spots. This technique is also used to see what transitional heat flux looks like under various perturbations. Heat flux data recorded by a dense array of sensors aligned in the spanwise direction (perpendicular to the flow) is used to form an image of the heat flux events crossing over the array. This image in the z-t plane (where z is spanwise distance and t is time), is essentially a 2-D time record of the surface heat flux across the span of the array. Figure 6 is an example of an image in the z-t plane showing the transitional heat flux events crossing a 40 mm span in less than 5 ms. The image not only shows intermittent heat flux, but it also captures the shape and structure of turbulent spots that appear in the laminar boundary layer.

The image in Figure 6 shows examples of fully developed spots having an arrowhead shape followed by a tail of relaxing heat flux. The fading tail is an effect of the calmed region, where the turbulent boundary layer relaxes back to a stable laminar profile. The image shown in Figure 6 was taken at a local Reynolds number of $Re_x = 2.4 \times 10^6$ under a favorable pressure gradient. No upstream turbulence grids were used in this particular case.

While images in the z-t plane are used to distinguish different turbulent spot shapes, images in the x-t plane are also acquired to track the growth and development of turbulent spots as they convect down the length of the plate. Figure 7 shows the surface heat flux recorded along a single streamwise array of films running straight down the center of the plate. The figure shows turbulent spots appearing towards the front of the plate. They

continue to grow as they convect downstream and eventually merge to form a fully turbulent boundary layer. For the case shown, the freestream velocity is 81 m/s and the Reynolds number based on the plate length of 332 mm is 1.8 x 10^6. This type of measurement has been used in the past to obtain turbulent spot leading and trailing edge velocities, and to measure the streamwise growth of turbulent spots. Turbulent spot propagation rates from the present experiments agree with and support earlier AFOSR sponsored tests by Clark (1993).

The high speed heat flux imaging technique can provide valuable information about turbulent spot generation and development, as well as show the effects of perturbations, such as freestream turbulence, pressure gradient and crossflow. A wealth of experimental data has been collected and is continuing to be analyzed. The following sections describe some early results.

Effects of Freestream Turbulence

Adding freestream turbulence causes transition to occur sooner and increases the overall heat flux to the surface. Figure 8 shows two segments of data taken at Re_x = 1.0 x10^5 under a freestream turbulence intensity *Tu* of 2.3% and zero pressure gradient. The images in the z-t plane show the heat flux events crossing a 7.2 mm span in just under 2.3 ms. Images of surface heat flux with this resolution in both space and time have been rare. The array is located just after the spot inception region, so spots appear smaller and less fully developed than those in Figure 6. The array is also further upstream where the boundary layer is thinner.

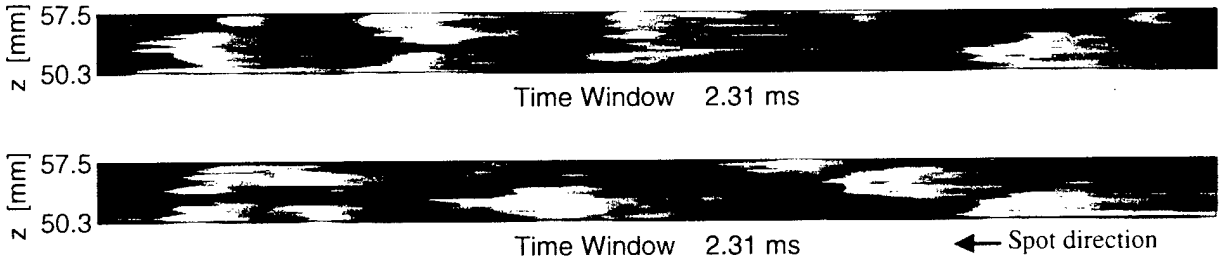

Figure 8 Turbulent spots induced by a freestream turbulence intensity of 2.3%. The image in the *z-t* plane shows heat flux events crossing a 7.2mm span in 2.31 ms.

Observations from these experiments also provide information about spot growth and development. It is found that the small initial turbulent vortices appear to induce additional turbulence slightly behind and to the side of each other forming an irregular patch of turbulent heat flux streaks. Given time to convect freely in this manner, the patch of turbulent vortices, known collectively as a turbulent spot, grows and develops into a regular arrowhead shape. A striated tail of calmed fluid follows behind the growing turbulent patch. In cases with considerable freestream turbulence, or where

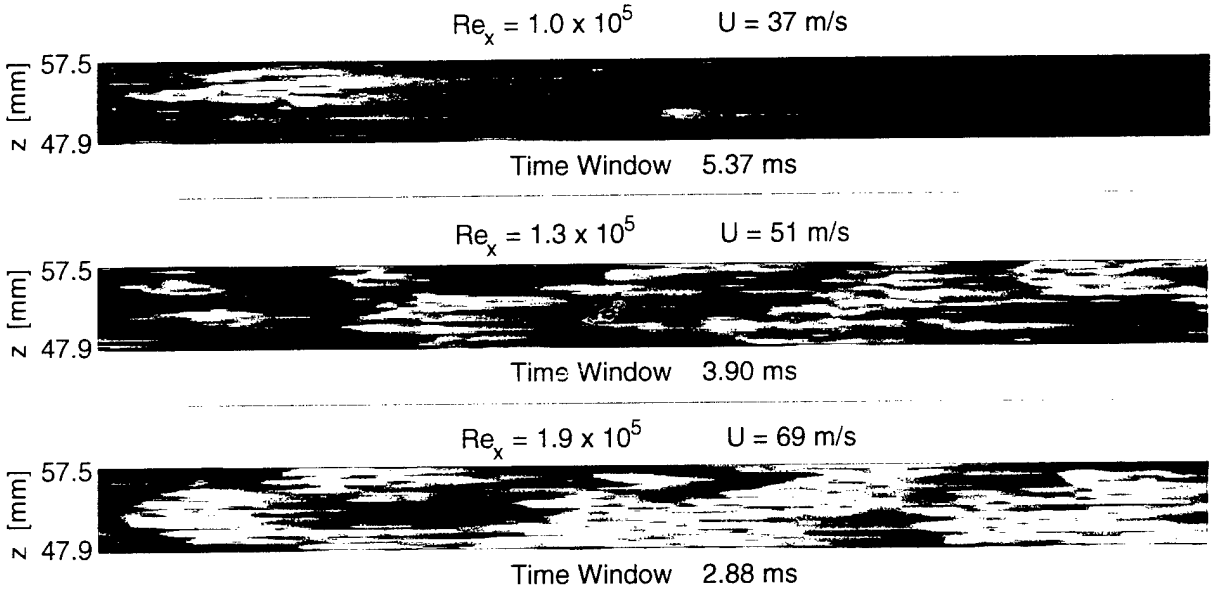

Figure 9 Images in the *z-t* plane showing increased turbulent intermittency as local Reynolds number is increased. Freestream turbulence intensity for each of these cases

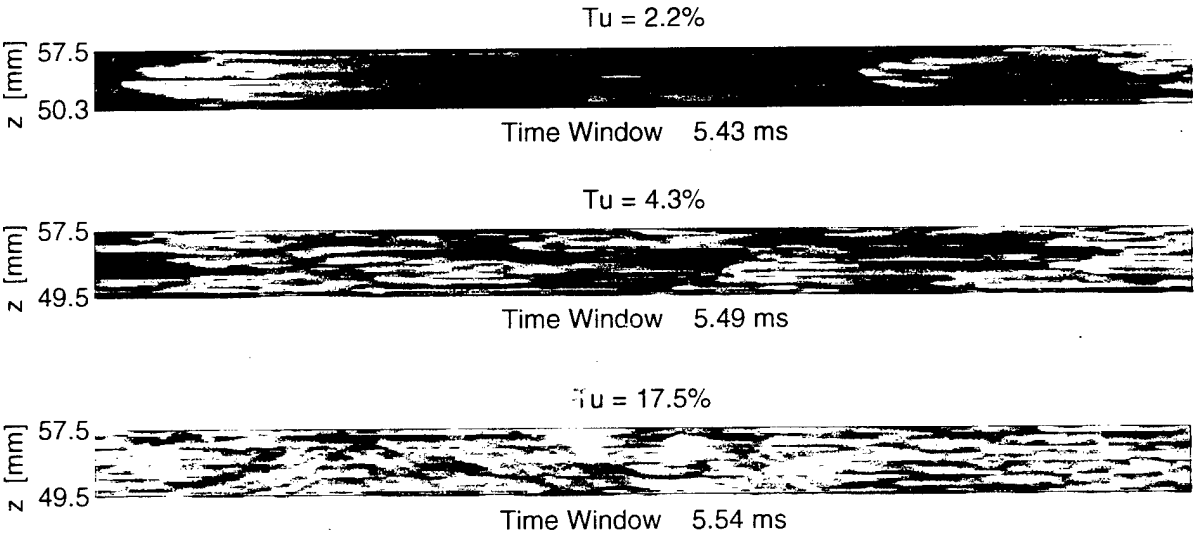

Figure 10 Effect of increasing freestream turbulence intensity. All images above were acquired at a set local Reynolds number of 1 x 10^5. Turbulence intensity was increased while attempting to hold the integral length scale constant

transition length is short, turbulent spots coalesce into a fully turbulent boundary layer before they are able to form the more developed classical arrowhead shape.

Figure 9 contains images from three different experiments showing the effect of increasing local Reynolds number. Data was taken at the same streamwise location at different freestream velocities. Upstream bar grids generated a freestream turbulence level of 2.3% in each case. As expected, increasing Reynolds number increases the

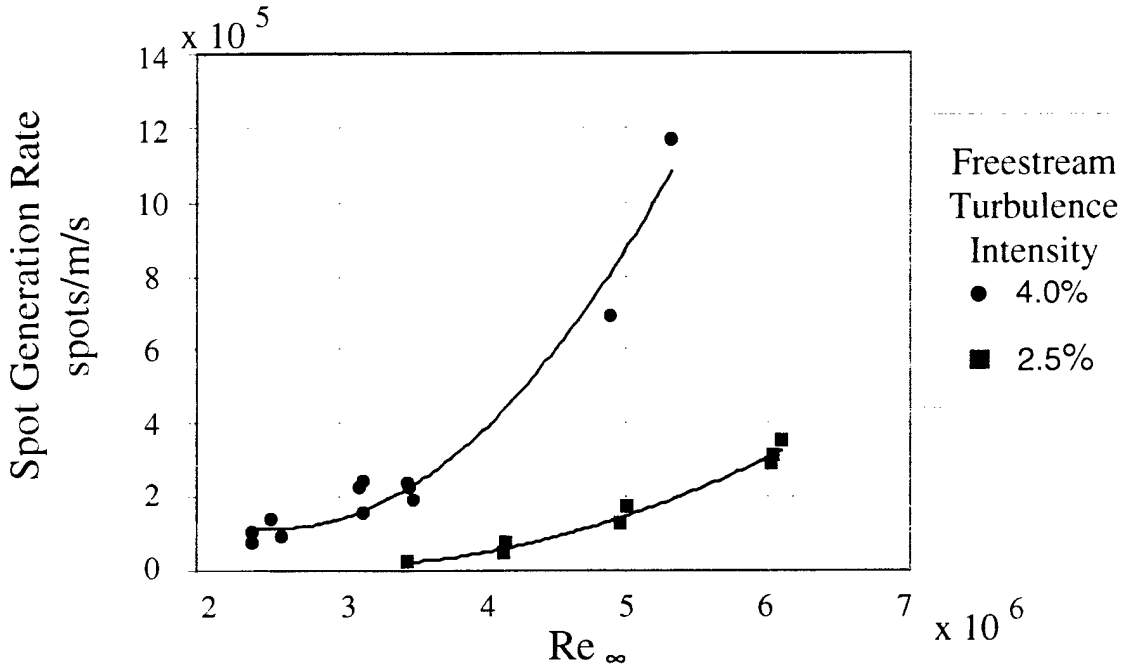

Figure 11 Direct Measurement of turbulent spot generation rate. Increasing Freestream turbulence significantly increases generation rate.

turbulent intermittency of the boundary layer, significantly increasing heat flux through the surface. This figure shows turbulent events growing and merging into a fully turbulent boundary layer.

Images of transitional heat flux at a fixed local Reynolds, but with increasing freestream turbulence intensity are shown in Figure 10. Different bar grid configurations were used to increase freestream turbulence intensity while attempting to hold the integral turbulent length scale constant. The images clearly show that increasing freestream turbulence intensity increases the number and complexity of turbulent spots seen at a given Reynolds number. It also shows the "streaky" nature of bypass transition caused by freestream turbulence. At a turbulence intensity level of 17.5%, the dominant heat transfer fluctuations are actually caused by the freestream eddies penetrating deep into the boundary layer. This type of data helps characterize the heat flux events occurring under appreciable levels of freestream turbulence. It is not clear that these are turbulent spots as they are conventionally envisaged.

The high speed heat flux imaging capability is valuable in that it also allows direct measurement of turbulent spot generation rate. Most methods infer generation rate from intermittency curves or use some other indirect method. The present technique allows one to distinguish between individual spots and count the number that pass over a spanwise length. Figure 11 shows measurements of spot generation rate over a range of Reynolds numbers under different turbulence intensities. Increasing freestream turbulence significantly increases the spot generation rate. Direct measurement of generation rate during naturally-occurring transition is valuable to those trying to realistically model transition.

Effects of Pressure Gradient

Along with freestream turbulence, experiments have also been performed to study the effects of adverse and favorable pressure gradients on transitional heat flux. A variable geometry test section was built to adjust the pressure gradient across the flat plate model. A simple sketch of an adverse pressure gradient is shown in Figure 12.

Under all but weak adverse pressure gradients, transition to turbulence was very abrupt without the appearance of isolated turbulent spots as seen earlier under zero pressure gradient flow. Relatively constant acceleration parameters of $K = -1 \times 10^{-7}$, -7×10^{-7}, and -10×10^{-7} were tested. The stronger adverse pressure gradients were found to cause a short laminar separation bubble that is transitional in the free shear layer and reattaches turbulent. Tests at $K = -7 \times 10^{-7}$ appear to separate at a Reynolds number of about 1.83×10^5 and reattach turbulent shortly after. Tests at $K = -10 \times 10^{-7}$ separate a little sooner, near a local Reynolds number of 1.69×10^5, and also reattach turbulent shortly downstream. This agrees with a previous AFOSR supported study on separated flow transition by Hatman and Wang (1998). Data plotted in Figure 13 appears to match previous data well, and falls into the region predicting laminar separation, short bubble transition.

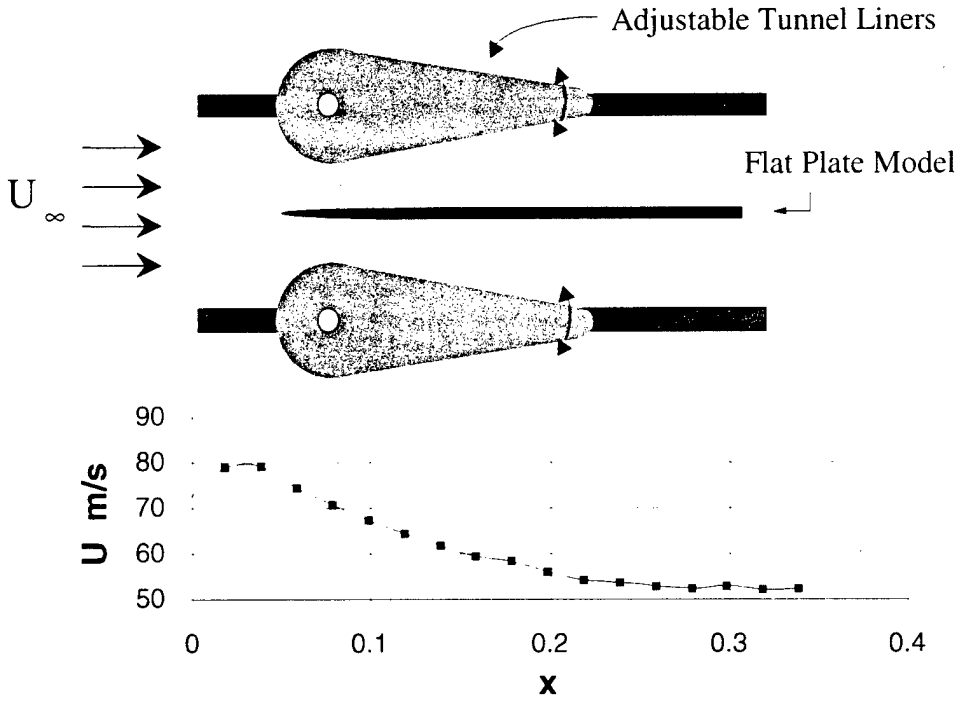

Figure 12 Adjustable test section geometry for study of adverse and favorable pressure gradients. A strong adverse pressure gradient is shown above.

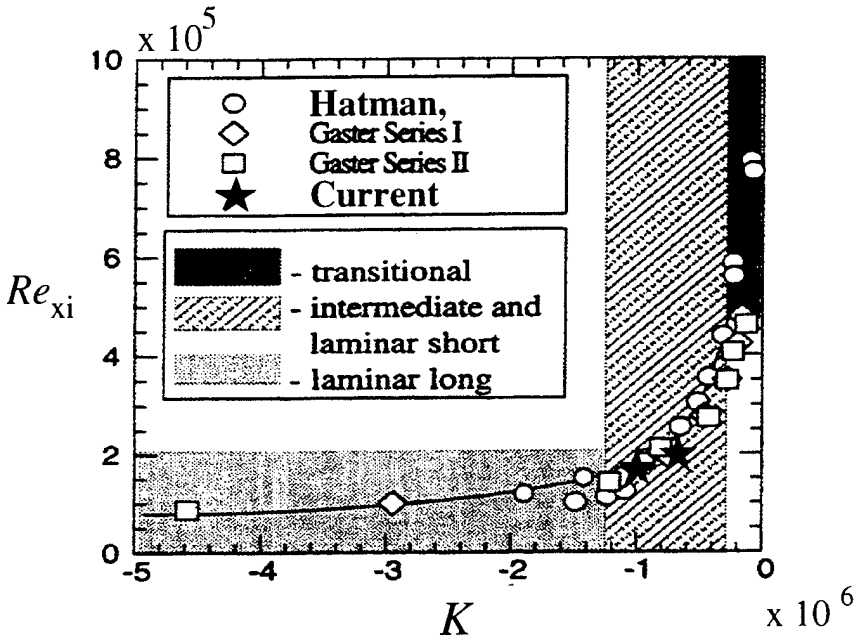

Figure 13 Transition onset under strong adverse pressure gradient compared with previous study by Hatman and Wang (1998). Data falls into region of laminar separation, short bubble transition.

Models of transitional heat flux under adverse pressure gradient must deal with various paths to turbulence. Since the laminar boundary layer can handle only a weak adverse pressure gradient, abrupt separated flow transition is very likely to occur. In this case, modelling the dynamics of individual turbulent spots may not be necessary nor even appropriate. However, when significant freestream turbulence (Tu=2% or more) is added, bypass transition occurs before separation, and individual turbulent streaks or spots do appear and rapidly coalesce. In this case of both strong adverse pressure gradient *and* freestream turbulence, a dynamic spot/streak model would still be appropriate and useful.

Table 1. Transition modes observed under adverse pressure gradient

Adverse Pressure Gradient	**Acceleration Parameter** $K = \frac{\nu}{U^2}\frac{dU_\infty}{dx}$	**Freestream Turbulence Intensity**	**Transition Mode**
Weak	-1×10^{-7}	< 1 %	Increased receptivity, natural transition before separation
Strong	-10×10^{-7}	< 1 %	Laminar separation / short bubble transition
Strong	-10×10^{-7}	4 %	***Bypass transition before separation***

Under very weak adverse pressure gradients, the boundary layer may remain attached, yet data shows the boundary layer has a greater receptivity to external perturbation. The increased receptivity usually leads to earlier transition. Table 1 lists some of the various modes of transition observed under both adverse pressure gradient and freestream turbulence.

Test section walls were also adjusted to study favorable pressure gradients. Favorable pressure gradients were generally found to delay transition onset, slightly reduce spot growth rate, and lengthen the transition region. Tests under favorable pressure gradient also revealed a stark difference between the growth rate of spots formed under natural transition, and the growth rate of bypass spots formed under significant freestream turbulence.

It was found that bypass spots (or streaks) which appear upstream at a lower Reynolds number do not grow as fast as natural spots that form later at higher Reynolds number. Figure 14 compares the growth of natural spots to bypass spots under a favorable pressure gradient. The figure plots the relative spot duration measured at each downstream location. Two cases are shown: one for natural transition, and another for bypass transition at a lower speed under 2.5% freestream turbulence intensity. The turbulence-induced spots (or streaks) formed at lower Reynolds number do not grow as fast as natural spots formed at higher Reynolds number. While many more streaky spots may be generated earlier under freestream turbulence, measurements show they do not grow much. The difference between natural and turbulence-induced spot growth is even more pronounced under the favorable pressure gradient because acceleration further stabilizes the boundary layer.

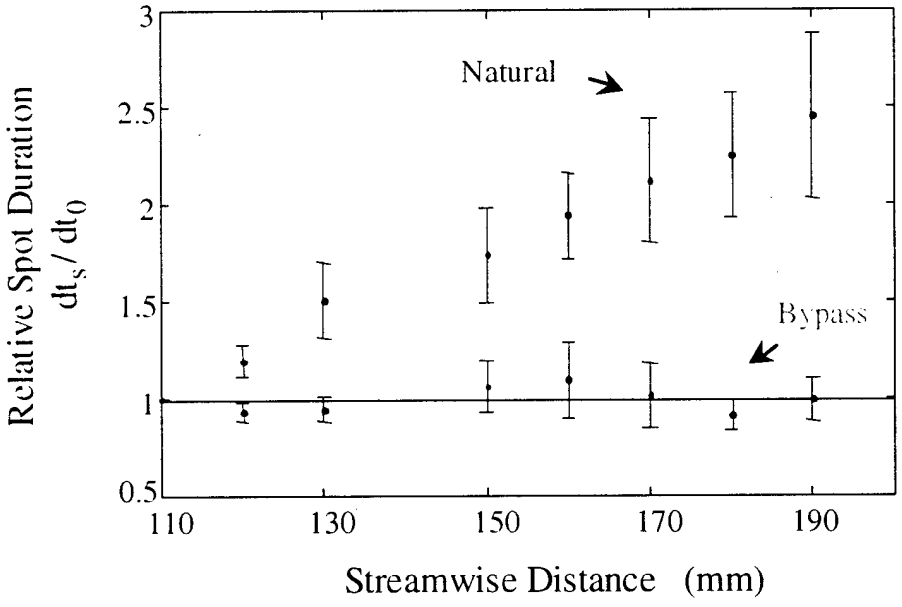

Figure 14 Comparison of natural vs. turbulence-induced spot growth under favorable pressure gradient. The bypass spots form at lower Reynolds number and do not grow as fast.

Effects of Crossflow

Crossflow occurs under a pressure gradient acting perpendicular to the inviscid streamline direction. Crossflow acceleration causes streamlines to curve over the surface producing a skewed 3-D boundary layer profile. This is illustrated in Figure 15. Crossflow occurs over many turbine surfaces including rotating components and rotor endwalls. Very little experimental research has been done however to study the effect of crossflow on transitional heat flux.

Experiments were performed using a contoured sidewall to turn the flow over the plate surface. Heat flux measurements show the crossflow pressure gradient destabilizes the boundary layer and causes transition to occur sooner, increasing the overall heat flux to the surface. Figure 16 is a comparison of surface heat flux measured along the plate surface both with and without crossflow. The figure plots the normalized heat flux traces from five downstream sensors. The crossflow measurements on the right were taken at lower Reynolds number under strong acceleration, both of which should stabilize the boundary layer and delay transition. But in this case, the acceleration is also in the spanwise direction inducing a skewed 3-D boundary layer. The crossflow effect dominates and quickly causes transition to turbulence.

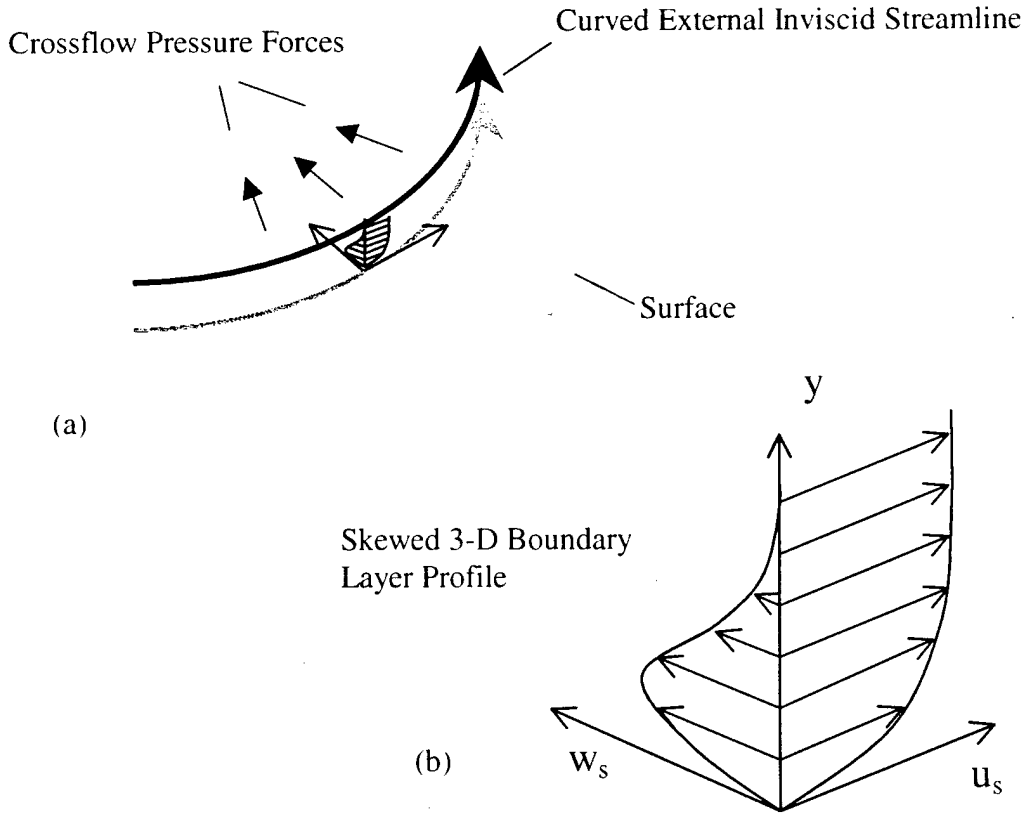

Figure 15 Streamlines are turned across the surface under a crossflow pressure gradient (a) resulting in a skewed three-dimensional boundary layer profile (b) that is inherently unstable.

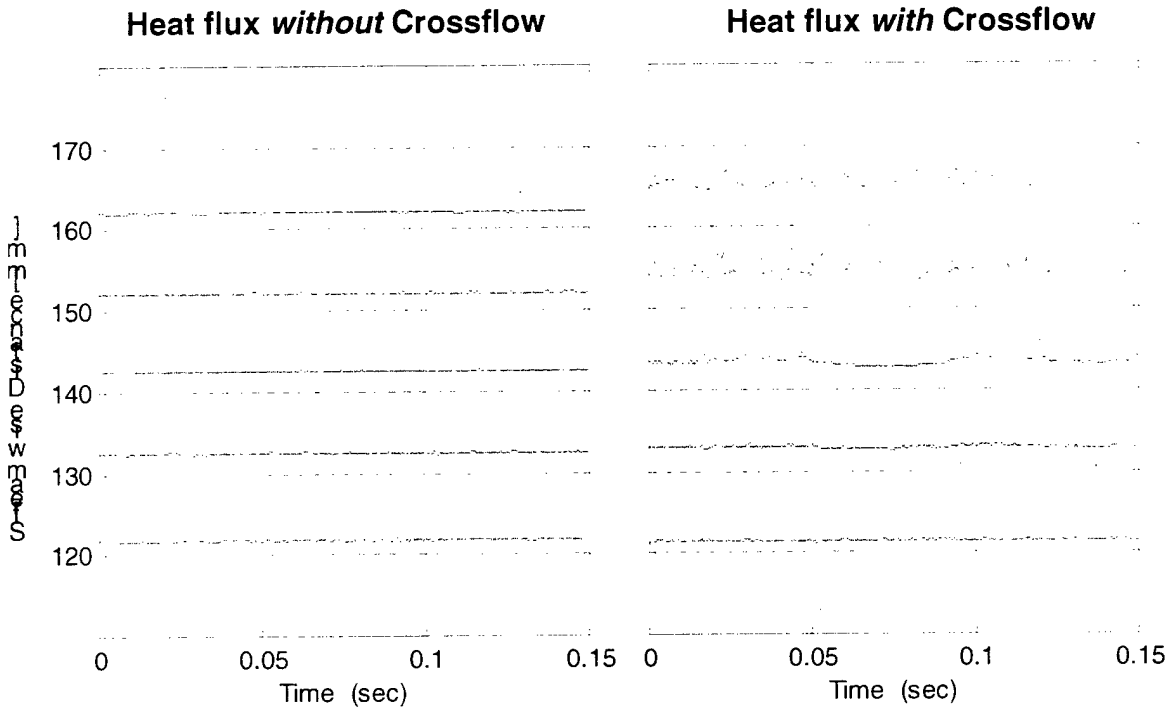

Figure 16 Comparison of boundary layer heat flux both with and without crossflow. The crossflow causes transition to occur sooner, even under a strong favorable pressure gradient and low Reynolds number.

Further investigation of surface heat flux under crossflow reveals both low frequency and high frequency instability waves. The low frequency waves appear first, followed by the appearance of a secondary instability having a wavelength an order of magnitude shorter. Similar observations have been made with crossflow over swept-back wings (Saric et. al. 1998, Bippes 1999). Measurements of the low frequency waves are compared with data from a swept wing study by Poll (1985) in Figure 17. Measurement of the non-dimensional frequency of the primary waves appears to agree.

High frequency heat flux images show the high and low frequency waves moving in two different directions. The images also show the aperiodic breakdown of secondary instability waves causes the strongest jumps in surface heat flux. The boundary layer then quickly becomes fully turbulent. It appears final transition occurs via the breakdown of these higher frequency waves.

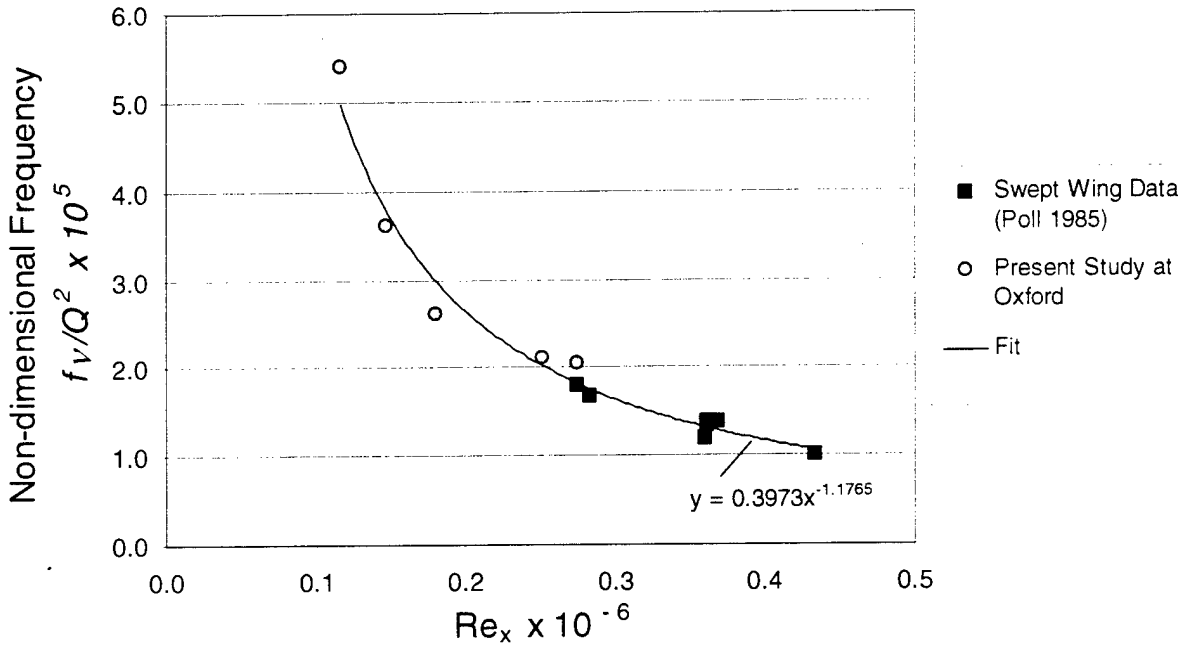

Figure 17 Comparison of measured primary travelling wave frequency with swept wing data measured by Poll (1985).

Conclusions

A high resolution surface heat flux imaging technique has been developed using high density thin film gauge arrays. The technique is used to capture detailed images of high speed transitional boundary layer heat flux. The heat flux imaging technique has been used in experiments to study the effects of freestream turbulence, pressure gradient, and crossflow.

High frequency, high spatial resolution detail has enabled direct measurement of turbulent spot generation rate, spot size, and spot/streak shapes. It is observed that individual spots do not always have a regular arrowhead shape as documented in past studies (Schubauer and Klebanoff 1955). Newborn spots and spots formed under appreciable freestream turbulence appear to have a streaky structure. The classical arrowhead shape may not actually appear in many cases; or in other words, it only forms under conditions where individual turbulent spots are allowed plenty of time to grow and fully develop before merging with any neighboring turbulence. Transition in turbines is likely to occur differently, due to the mix of freestream turbulence, pressure gradients, crossflow, and other boundary layer disturbances.

Experiments were performed to study the effect of freestream turbulence, pressure gradient, and crossflow on transitional heat flux. Increasing freestream turbulence intensity causes transition to occur further upstream at a lower Reynold's number. Turbulence-induced spots are very streaky in nature and do not appear to grow as much

as normal spots formed at higher Reynolds number. Direct measurements of spot generation rate also show freestream turbulence intensities above 1% substantially increase the number of spots generated per meter per second.

Varying pressure gradients can drastically alter the path to turbulence. Separated flow transition is likely to occur under adverse pressure gradient. This is often a very abrupt transition that does not involve propagation of turbulent spots along the surface. Under weak adverse pressure gradients, the boundary layer may not separate, but it has an increased receptivity to external perturbations that may cause early transition. Favorable pressure gradients have the opposite effect of delaying transition, reducing spot growth, and lengthening the transition region.

Transition under crossflow also does not involve the type of spot development seen under straight zero pressure gradient flow. Crossflow induces a skewed 3-D boundary layer that becomes unstable and breaks down into a turbulent boundary layer. Crossflow has a dominant effect that causes transition to occur even at low Reynolds number and under a strong favorable acceleration. Heat flux signals reveal both low frequency and high frequency travelling waves, which agree with studies of crossflow over swept-back wings. High frequency heat flux images suggest transition occurs via intensification and breakdown of the higher frequency waves. The boundary layer then quickly becomes fully turbulent.

A large amount of experimental data has been collected under this study and is continuing to be analyzed and documented. New information from these experiments may eventually be used to improve our understanding of transition in complex flows, and enable more accurate prediction of transitional heat transfer in turbines.

Acknowledgement/Disclaimer

This work was sponsored (in part) by the Air Force Office of Scientific Research, USAF, under grant/contract number F49620-97-1-0524, technical monitor Dr. Tom Beutner. The views and conclusions contained herein are those of the authors and should not be interpreted as necessarily representing the official policies or endorsements, either expressed or implied, of the Air Force Office of Scientific Research or the U.S. Government.

Personnel Supported

Richard J. Anthony Doctorate Student, University of Oxford, U.K.

References

Ainsworth, R.W., Allen, J.L., Davies, M.R., Forth, C.J.P., Hilditch, M.A., Oldfield, M.L.G. and Sheard, A.G., 1989, "Developments in Instrumentation and Processing for Transient Heat Transfer Measurements in a Full-Stage Model Turbine", *ASME J. Turbomachinery*, vol. 111 pp. 20-27.

Anthony, R.J., 2001, *Turbulent Spot Characterization and the Investigation of Transitional Heat Transfer in Turbines*, D.Phil. Thesis, Department of Engineering Science, Oxford University, U.K.

Anthony, R.J., Jones, T.V., LaGraff, J.E., 2001 "Visualization of High Speed Transitional Boundary Layer Heat Flux using High Density Thin Film Arrays", Presented at *39th AIAA Aerospace Sciences Meeting and Exhibit*, 8-11 January 2001, Reno, NV. Paper No. AIAA-2001-0553.

Anthony, R.J., Jones, T.V., LaGraff, J.E., 2000. "Visualization of transitional heat flux in the presence of freestream turbulence and pressure gradient," *Proceedings of the Minnowbrook III Workshop on Transition in Turbomachines*, to be published in NASA Conference Proceedings Report.

Anthony, R.J., M.L.G. Oldfield, Jones, T.V., J.E. LaGraff, 1999, "Development of High-Density Arrays of Thin Film Heat Transfer Gauges," *Proceedings of the 5th ASME/JSME Thermal Engineering Joint Conference*, San Diego, CA. Paper No. AJTE99-6159.

Bippes, H., 1999. "Basic experiments on transition in three-dimensional boundary layers dominated by crossflow instability," *Progress in Aerospace Sciences* 35, pp.363-412.

Clark, J.P., 1993, *A Study of Turbulent-Spot Propagation in Turbine Representative Flows*, D.Phil. Thesis, Department of Engineering Science, University of Oxford, U.K.

Clark, J.P., Jones, T.V., and LaGraff, J.E., 1993, 'On the Propagation of Naturally-Occurring Turbulent Spots," *Journal of Engineering Mathematics*, special issue on turbulent spots, ed. F.T. Smith.

Dunn, M.G., 1989, "Phase and Time Resolved Measurements of Heat Transfer and Pressure in a Full-Stage Rotating Turbine", ASME, paper 89-GT-135.

Epstein, A.H., Guenette, G.R., Norton, R.J.G. and Yuzhan, G., 1986, "High Frequency Response Heat Flux Gauges", Rev. Sci. Instrum., 57 (4), pp 639-649.

Hatman, A., and Wang, T., 1998, "A Prediction Model for Separated-Flow Transition," ASME Paper 98-GT-237.

Hofeldt, A., 1993, *The Investigation of Naturally-Occurring Turbulent Spots Using Thin-Film Gauges*, D.Phil. Thesis, Department of Engineering Science, Oxford University, U.K.

Kimura, M.S. Tung, J. Liu, C.M. Ho, F. Jiang and Y.C. Tai, 1998, "Measurements of Wall Shear Stress of Turbulent Boundary Layer Using Micro Shear Stress Imaging Chip," Journal of Japan Soc. of Mech. Eng.

Kittichaikarn, C., Ireland, P.T., Zhong, S., Hodson, H.P., 1999, "An investigation on the onset of wake-induced transition and turbulent spot production rate using thermochromic liquid crystals," Proceedings, ASME International Gas Turbine and Aeroengine Congress and Exhibition, Indianapolis, IN, USA, ASME Paper 99-GT-126.

Mayle,R.E., 1991, "The Role of Laminar-Turbulent Transition in Gas Turbine Engines", *ASME J. Turbomachinery*, Vol. 112, pp. 188-195.

Oldfield, M.L.G., 2000, "Guide to Impulse Response Heat Transfer Signal Processing: Version 2", Oxford University Engineering Lab Report 2233/2000.

Oldfield, M.L.G., Burd, H.J. and Doe, N.G., 1982, "Design of Wide-Bandwidth Analogue Circuits for Heat Transfer Instrumentation in Transient Tunnels," Proc. 14th *ICHMT Symposium on Heat and Mass Transfer in Rotating Machinery*, Dubrovnik.

Poll, D.I.A., 1985. "Some observations of the transition process on the windward face of a long yawed cylinder," *J. Fluid Mech.*, Vol. 150, pp.329-356.

Roach, P.E., 1987, "The generation of nearly isotropic turbulence by means of grids," Journal of Heat and Fluid Flow, vol. 8, No.2.

Saric, W.S., Carrillo, R.B., Reibert, M.S., 1998. "Nonlinear stability and transition in 3-D boundary layers," *Meccanica*Vol. 33, 1998, pp.469-487.

Schubauer, G.B. and Klebanoff, P.S., 1955, "Contributions on the Mechanics of Boundary Layer Transition," NASA TN-3489.

Schultz, D.L. and Jones, T.V., 1973, "Heat Transfer Measurements in Short-Duration Hypersonic Facilities," AGARD AG-165.